Optical–Optical Double-Resonance Spectroscopy of the $1_u(^3P_2)$ and $2_u(^3P_2)$ States of I_2 Through the $A^3\Pi(1_u)$ State

Takashi Ishiwata,* Satoshi Motohiro, Eriko Kagi, Hisashi Fujiwara, and Masaru Fukushima

Department of Information Machines and Interfaces, Faculty of Information Sciences, Hiroshima City University, Ozukahigashi, Hiroshima 731-3194

(Received May 10, 2000)

Optical-optical double-resonance spectroscopy is used to study the $1_u(^3P_2)$ and $2_u(^3P_2)$ ion-pair states of I_2 correlating to the lowest ionic state, $I^-(^1S)+I^+(^3P_2)$. In the (1+2) photoexcitation sequence, we gain access to the $1_u(^3P_2)$ ion-pair state through the $A^3\Pi(1_u)$ state. The $2_u(^3P_2)$ state is also identified from the occurrence of extra lines through heterogeneous coupling with the $1_u(^3P_2)$ state and an apparent energy shift in the $1_u(^3P_2)$ state. The energy levels of the $1_u(^3P_2)$ and $2_u(^3P_2)$ states were analyzed in detail by including the heterogeneous interaction between these states. We have established the vibrational numbering of the $2_u(^3P_2)$ state in considering the 1_u–$2_u(^3P_2)$ interaction terms under a pure precession approximation. Combined with other results, the present study has allowed us to characterize and map out the ion-pair states of I_2 in the 5 eV region.

The interaction $I^+(^3P)+I^-(^1S)$ gives rise to twelve ionic states, which form two clusters of six states corrresponding to the energies of the fine-structure components of the I^+ ion ($^3P_2$ and $^3P_{1,0}$). The mean energy of the lowest cluster (0_u^+, 1_u, 2_u, 0_g^+, 1_g and $2_g(^3P_2)$) is about 41000 cm^{-1} above the $X^1\Sigma_g^+$ ground state, and the second (0_u^-, 1_u 0_g^-, and $1_g(^3P_1)$; 0_u^+ and $0_g^+(^3P_0)$) is located at around 47000 cm^{-1}.[1] Since these states can not be accessed directly from the ground state, due to the optical selection rules and the Franck–Condon principle, the optical-optical double-resonance technique has usually been used to characterize them.

Rousseau and Williams first demonstrated a stepwise approach to the $0_g^+(^3P_2)$ state through the $B^3\Pi(0_u^+)$ state.[2] Danyluk and King developed this technique using two tunable dye lasers, and showed the ability to explore the excited states systematically in the (1+1) photo-excitation sequence.[3] They observed the five excited states in the 40000—42000 cm^{-1} range, which were labelled as α, β, γ, δ, and ε in order of increasing frequency of the first observed lines. An experiment of this type has been repeated many times. These results show that the states, ε, β, and α, are three *gerade* states ($0_g^+(^3P_2)$, $1_g(^3P_2)$, and $2_g(^3P_2)$) correlating to the lowest ionic state of $I^+(^3P_2)+I^-(^1S)$, respectively.[4—11]

The other two states (γ and δ) remaining unassigned are, therefore, suggested to have some of the *ungerade* states correlating to the same asymptote.[12] In view of the optical selection rules for homonuclear diatomic molecules, the observations of the *ungerade* states are peculiar in the (1+1) photo-excitation sequence from the $X^1\Sigma_g^+$ ground state. This was interpreted as a phenomenon that the *ungerade-gerade* character broke in the $B^3\Pi(0_u^+)$ intermediate state through hyperfine coupling with a 1_g state which shares the same dissociation limit, $^2P_{1/2}+^2P_{3/2}$.[13] The $0_u^+(^3P_2)$ state was observed through the $0_u^+(^3P_2)$–$X^1\Sigma_g^+$ transition and the $0_u^+(^3P_2)$–$B^3\Pi(0_u^+)$–$X^1\Sigma_g^+$ multiphoton ionization spectra.[14,15] Ishiwata and Tanaka recently analyzed this state by optical-optical double-resonance in the (1+2) photo-excitation sequence through the $B^3\Pi(0_u^+)$ state.[16] The $0_u^+(^3P_2)$ state was known to be different from any states found by Danyluk and King. Consequently, through an elimination process, the γ and δ states are now believed to be the $1_u(^3P_2)$ and $2_u(^3P_2)$ states, respectively, while there was insufficient data to establish the assignments until now.

In the present paper we report on some new experimental results to answer this problem in a straightforward manner. Since the valence to ion-pair state transition has a charge transfer property along the internuclear axis, we are able to probe the $\Delta\Omega = 0$ transition. The $1_u(^3P_2)$ state can be reached as the final state of the double-resonance, $1_u(^3P_2)$–$A^3\Pi(1_u)$–$X^1\Sigma_g^+$, using the coherent two-photon transition from the $A^3\Pi(1_u)$ state. Appadoo et. al have recently analyzed the $A^3\Pi(1_u)$—$X^1\Sigma_g^+$ absorption spectrum of I_2 in the near-infrared region,[17] and provided reliable data for carrying out a double-resonance experiment through the $A^3\Pi(1_u)$ state. This technique allowed us to resolve the rotational structures of the $1_u(^3P_2)$ state with state selection in the intermediate $A^3\Pi(1_u)$ state. All observed transitions followed the $\Delta\Omega = 0$ propensity rule, and consisted of the O, Q, and S rotational lines. The $2_u(^3P_2)$ state was also found through $1_u(^3P_2)$—$2_u(^3P_2)$ heterogeneous mixing. This study clarified the symmetrical properties of the ion-pair states in view of the optical selection rules, and provided a firm basis for describing the $1_u(^3P_2)$ and $2_u(^3P_2)$ states.

Experimental

In the presently described experiments, we aimed to analyze the energy levels of the $1_u(^3P_2)$ state by optical–optical double

resonance using the (1+2) photo-excitation sequence through the $A^3\Pi(1_u)$ state:

$$1_u(^3P_2) \xleftarrow{2h\nu_2} A^3\Pi(1_u) \xleftarrow{h\nu_1} X^1\Sigma_g^+, \quad (1)$$

where each transition component satisfies the symmetrical selection rules: $g \leftrightarrow u$ for one-photon transitions and $g \leftrightarrow g$ (or $u \leftrightarrow u$) for two-photon transitions.

For double-resonance excitation, we used two tunable lasers pumped by the outputs of a Nd:YAG laser operated at 10 Hz. One laser (Lambda Physik ScanMate OPPO E), referred to as the "pump" laser, was an opto-parametric oscillator seeded with the radiation of a narrow-band pulsed dye laser excited by the third-harmonic output. This laser was operated at a fixed frequency (ν_1) to excite the I_2 molecules from the $X^1\Sigma_g^+$ ground state to the $A^3\Pi(1_u)$ state by idler light in the near-infrared region. An undesired visible output was removed by passing the laser beam through a sharp cut-off filter. The other laser (Scanmate 2E), a "probe" laser, excited by the second harmonics was operated in the visible region and scanned to survey the ion-pair states in a coherent two-photon transition. Both tunable lasers produced pulses with an energy of 2—5 mJ/pulse. There was a 5 ns delay between two laser pulses having a 7 ns duration. The sample pressure was about 0.2 Torr (1 Torr = 133.322 Pa), which was sufficiently low to exclude any collisional relaxation in the intermediate state. The bandwidth of the tunable lasers was 0.02 cm^{-1} in the case of operating with an intracavity étalon, and 0.2 cm^{-1} without the étalon. The probe laser frequency (ν_2) was calibrated by reference to the I_2 $B^3\Pi(0_u^+)$–$X^1\Sigma_g^+$ absorption spectrum, and determined with an estimated accuracy of better than 0.01 cm^{-1}.

Both laser beams were aligned to counterpropagate in a parallel fashion, and focussed on the same spot. The double-resonance transitions were detected by monitoring the emission to the lower valence states through an interference filter (λ = 480±10 nm). Photomultiplier signals were integrated by a boxcar.

Results and Discussion

A. Double-Resonance Transitions to the Ion-Pair States: Figure 1 shows the typical double-resonance spectrum observed in the experiment. It was obtained by adjusting the pump laser frequency (ν_1) to a photon energy of 11500.6 cm^{-1}, which was in resonance with the $A^3\Pi(1_u)$—$X^1\Sigma_g^+$ (18-2)Q_{40} and (25-3)Q_{33} transitions. Since excitation occurs through the restricted rovibronic levels, the obtained spectrum is drastically simplified. These spectra can be interpreted and analyzed by following the comments concerning the excitation processes and the rotational selection rules for the two transition components.

The $A^3\Pi(1_u)$—$X^1\Sigma_g^+$ system is perpendicular, obeying the rotational selection rules of $\Delta J = 0$ and ±1. Figure 2 shows the spectrum obtained by scanning the pump laser, while the probe laser was fixed to a photon energy of 15081.3 cm^{-1}, which is resonant to the $1_u(^3P_2)$–$A^3\Pi(1_u)$ (6-18)Q_{40} in Fig. 1. Fortunately, the rotational constants of two states are very close in the $1_u(^3P_2)$–$A^3\Pi(1_u)$(6-18) transition. The probe laser excited the Q branches of the probe transition over a wide J range, and labeled the intermediate $A^3\Pi(1_u)$ $v = 18$ state. Consequently, we could determine the pump transition, as shown in spectrum (a) of Fig. 2. The pump transition has the P/Q/R triplet structures characteristic of

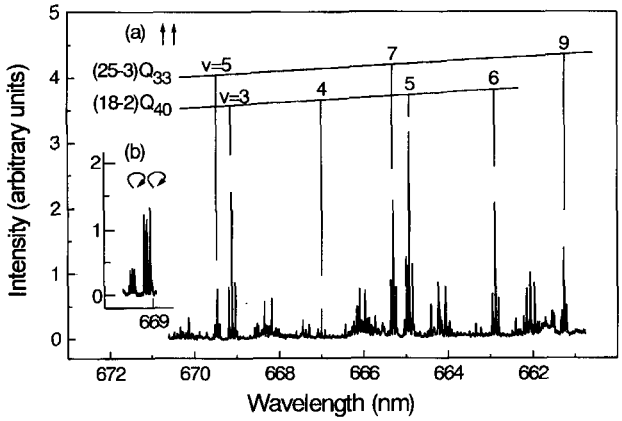

Fig. 1. Optical–optical double-resonance spectra of I_2 excited to the $1_u(^3P_2)$ ion-pair state through the $A^3\Pi(1_u)$—$X^1\Sigma_g^+$ (18-2)Q_{40} and (25-3)Q_{33} transitions. The probe laser was scanned with the (a) linearly and (b) circularly polarization. The Franck–Condon factors (×10^3) of the $1_u(^3P_2)$—$A^3\Pi(1_u)$ transition originating from the $A^3\Pi(1_u)$ (a) $v = 18$ $J = 40$ and (b) $v = 25$, $J = 33$ states are calculated as:

$A^3\Pi(1_u)$ \ $1_u(^3P_2)$	$v = 3$	4	5	6	7	8	9
(a)	59.5	3.9	155.5	55.1	0.1	21.6	109.7
(b)	1.4	1.7	23.5	3.0	86.6	0.2	31.8

the $A^3\Pi(1_u)$—$X^1\Sigma_g^+$ transition, which is more obvious in spectrum (b) taken under higher resolution. Even though the intensity ratio of the P/Q/R branches is not 1 : 2 : 1, probably due to saturation, we can easily assign the spectrum as the (18-2) band of the $A^3\Pi(1_u)$–$X^1\Sigma_g^+$ system from their known spectroscopic constants.[17] The transitions originating from the $X^1\Sigma_g^+$ $v = 1$ and 3 states were, of course, found at different wavelength regions, and we confirmed that the excitation to the ion-pair state occurs through the $A^3\Pi(1_u)$ state. The multiple pumping in the $A^3\Pi(1_u)$—$X^1\Sigma_g^+$ transition usually occurred within the laser bandwidth. However, it caused no problem to analyze the spectra.

The $1_u(^3P_2)$—$A^3\Pi(1_u)$ system follows the selection rules $\Delta J = 0$, ±1, and ±2 for the two-photon transitions between the states of $\Delta\Omega = 0$, while the P and R branches only occur when J is quite small. Spectrum (a) in Fig. 1, taken by a probe laser with linear polarization, obviously shows the O, Q, and S triplet with the 1 : 3 : 1 intensity ratio. On the other hand, in spectrum (b) taken by a circularly polarized probe laser, the intensity ratio changes to the 1 : 1 : 1 ratio. At that time the O and S lines increase in intensity and increase to one half times as much as those in spectrum (a). According to a theoretical treatment on a coherent two-photon transition, this polarization behavior is characteristic of the transition executed by two identical photons,[18] indicating that the two-photon transition occurs from the $A^3\Pi(1_u)$ state by the probe laser alone. Consequently, the progressions designated the $1_u(^3P_2)$ state as a terminus have the vibrational intervals of ca. 94 cm^{-1}. Since their absolute positions are fairly consistent with those of the γ state reported by King et al.,[4] we followed their vibrational numbering, as described later.

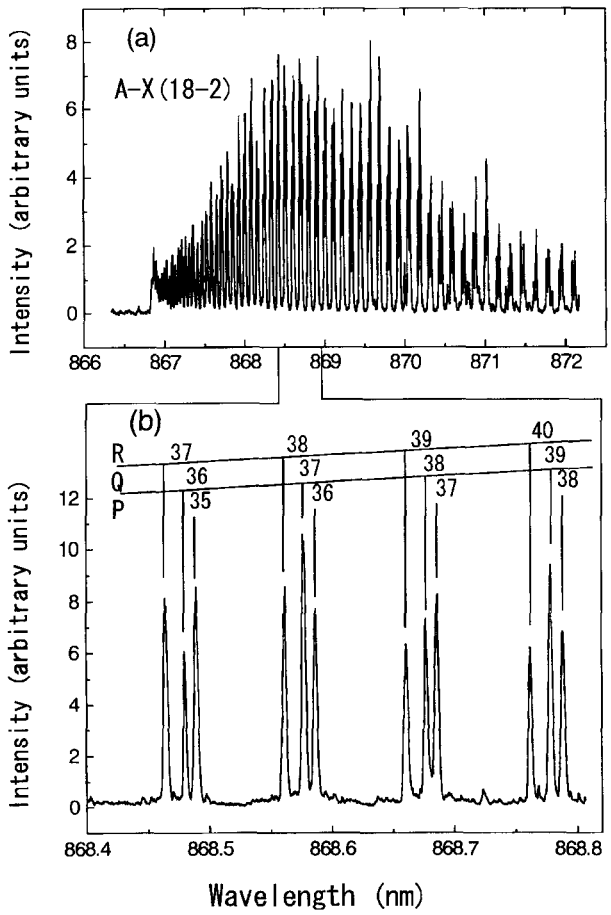

Fig. 2. Optical–optical double-resonance spectra showing the (18-2) band of the $A^3\Pi(1_u)$–$X^1\Sigma_g^+$ system. The probe frequency was adjusted to a photon energy of 15081.3 cm^{-1}, which is in resonance with the Q branches of the (6-18) vibrational band in the $1_u(^3P_2)$–$A^3\Pi(1_u)$ system in the wide range of J. The pump laser was scanned with (a) 0.2 cm^{-1} and (b) 0.02 cm^{-1} resolution.

It should be noted that there remained many unassigned bands in the spectrum of Fig. 1, most of which occurred only by the probe laser. These bands might be attributed to the transitions to the $0_u^+(^3P_2)$ or $0_u^+(^3P_1)$ ion-pair states through the $B^3\Pi(0_u^+)$ state due to an accidental matching of the probe laser frequency to the $B^3\Pi(0_u^+)$—$X^1\Sigma_g^+$ and $0_u^+(^3P_2)$—$B^3\Pi(0_u^+)$ transitions in the (1+2) photo-excitation; they were excluded in the analysis.

The $A^3\Pi(1_u)$ and $1_u(^3P_2)$ states are both degenerated. In a one-photon transition, the pump transition combines the upper e sublevels of the $A^3\Pi(1_u)$ state with the $X^1\Sigma_g^+$ ground state through the P and R branches, while the lower f sublevels through the Q branches, according to the parity selection rules ($e\leftrightarrow f$). On the other hand, in the two-photon transition, the probe transition allows either an $e\leftrightarrow e$ or $f\leftrightarrow f$ transition between the $1_u(^3P_2)$ and $A^3\Pi(1_u)$ states. We can therefore select and probe either the e or f sublevels of the $1_u(^3P_2)$ state, depending on whether the molecules are pumped to the v, J level of the $A^3\Pi(1_u)$ state through a P (or R), or a Q branch of the $A^3\Pi(1_u)$–$X^1\Sigma_g^+$ transition, respectively.

B. Analysis: For analyzing the $1_u(^3P_2)$ state, the term values were calculated from the following three quantities: (i) the term value of the initial ground state; (ii) the frequency of the pump transition, $A^3\Pi(1_u)$–$X^1\Sigma_g^+$; and (iii) the frequency of the probe transition. The first two quantities required for the sum were derived from the known spectroscopic constants of the $X^1\Sigma_g^+$ and $A^3\Pi(1_u)$ states. The present experiment provides a third with an estimated accuracy of 0.01 cm^{-1}. The raw data include 606 transitions in the $0\leq v\leq 11$ and $5\leq J\leq 119$ ranges for the $1_u(^3P_2)$ state.** During excitation, the molecules gain their own Franck–Condon region depending on the vibrational levels of the intermediate state. The observed vibrational progression shows a modulation pattern characteristic to the intermediate state, as shown in Fig. 1. We should use the vibration levels of the intermediate $A^3\Pi(1_u)$ state spanning from $v=11$ to 20 to cover the $1_u(^3P_2)$ state up to $v=11$.

The probe laser frequency (ν_2) was converted to the energy relative to the potential minimum of the ground state;

$$T_{v,J} = T_{v^*,J^*}(A) + 2h\nu_2, \quad (2)$$

where $\Delta J = J - J^* = 0, \pm 2$. The term values of the $A^3\Pi(1_u)$ state, $T_{v^*,J^*}(A)$, from which the two-photon transition originated were calculated from the constants given by Appadoo et al.[17] Even though the present data do not cover all rotational levels, they are sufficient to determine the centrifugal distortion of the observed vibrational states and the Ω-doubling.

Figure 3 shows our data of the first vibrational level of the $1_u(^3P_2)$ state. It lies at 41668.747(33) cm^{-1} above the

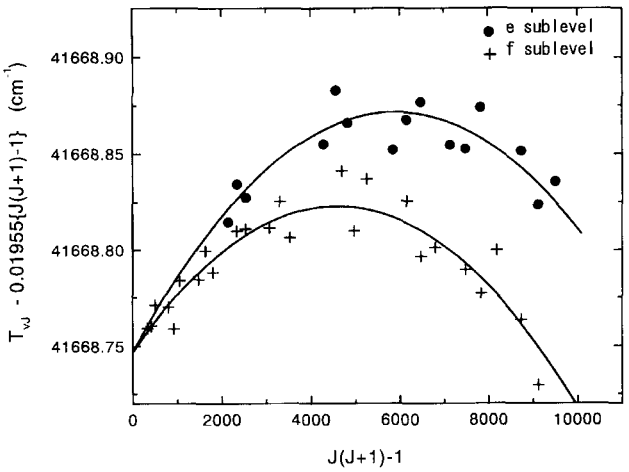

Fig. 3. Energy level diagram of the $1_u(^3P_2)$ $v=0$ state. (●) denotes the e sublevels of the $1_u(^3P_2)$ state, and (+) denotes the f sublevels. The solid curves show the unperturbed energy levels of the ion-pair state with the molecular constants of $T_0 = 41668.747(6)$ cm^{-1}, $B_0^f = 0.0195830(26)$ cm^{-1}, $D_0 = 3.59(64)\times10^{-9}$ cm^{-1}, and q_0 ($= B_0^e - B_0^f$) = $9.31(64)\times10^{-6}$ cm^{-1}, where the numbers in parentheses denote one standard deviation.

** The frequency table is available from the authors.

potential minimum of the ground state with the rotational constant of 0.0195830(26) cm^{-1} for the *f* sublevels, which is close to the observation for the γ $v = 0$ state by King et al.[4] Our data cover the vibrational levels up to $v = 11$, all of which are located at the energies anticipated from the γ state within 0.7 cm^{-1}. King et al. determined the vibrational numbering of the γ state from the isotope shifts of the vibrational energies between $^{127}I_2$ and $^{129}I_2$. Jewsbury et al. lately accessed the γ state following the procedure of King et al. and confirmed their vibrational numbering from the modulation patterns of the $1_u(^3P_2)$-c1_g emission at 460 nm in view of the Franck–Condon factor calculations.[19] There is no doubt to conclude that γ is the $1_u(^3P_2)$ state, and we have vibrationally numbered the $1_u(^3P_2)$ state according to the result of the γ state.

Our data also involve the transitions terminating on the $2_u(^3P_2)$ state. The transition from the valence to the ion-pair state is paralell, which imposes the $\Delta\Omega = 0$ selection rule. The $2_u(^3P_2)$–$A^3\Pi(1_u)$ transition is therefore symmetrically forbidden. The $2_u(^3P_2)$ state is only detected in the spectrum by intensity borrowing, resulting from mixing of the wavefunctions with the $1_u(^3P_2)$ state. Consequently, the transitions to the $2_u(^3P_2)$ state were observed in the extra lines consisting of O/Q/S triplet identical to those to the $1_u(^3P_2)$ state transition, whose example is shown in Fig. 4. This spectrum was observed during an analysis of the $1_u(^3P_2)$ $v = 5$ state. Two sets of transitions with the O, Q, and S branches lie about 1 cm^{-1} apart. The weaker components, located at lower energies, lost their intensity along with an increase of *J*. Two adjacent states are degenerated, since we detected them by pumping the molecules through the P (or R) and Q branches of the $A^3\Pi(1_u)$—$X^1\Sigma_g^+$ transition. Figure 5 summarizes the energy levels found in this energy range. It is easy to understand that the $2_u(^3P_2)$ state lies below the $1_u(^3P_2)$ $v = 5$ state, and that its rotational constant is smaller than that of the $1_u(^3P_2)$ state. The mixing coefficient should be sensitive to the variation of *J*. Even though the magnitude of the interaction matrix element is nearly proportional to *J*, the $2_u(^3P_2)$ state become rapidly separate from the $1_u(^3P_2)$ state along with an increase of *J*. We failed to detect the $2_u(^3P_2)$ state through heterogenous 1_u–$2_u(^3P_2)$ mixing at higher *J* levels.

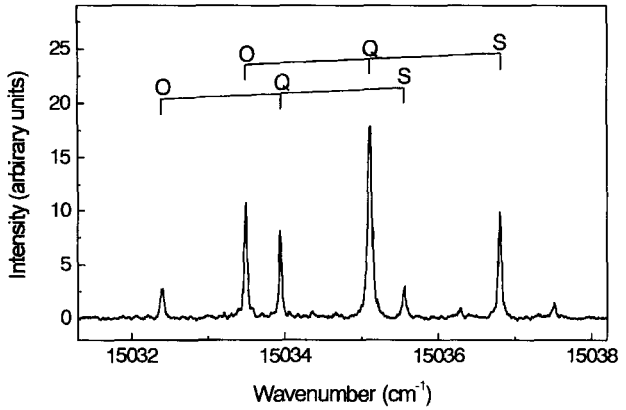

Fig. 4. Optical–optical double resonance spectrum taken under high resolution (0.02 cm^{-1}). The pump laser was adjusted to the (18-3)R_{41} branch of the $A^3\Pi(1_u)$—$X^1\Sigma_g^+$ system. The probe laser was scanned in the energy region of the $1_u(^3P_2)$ $v = 5$ state, where the $2_u(^3P_2)$ $v = 3$ state lies closely.

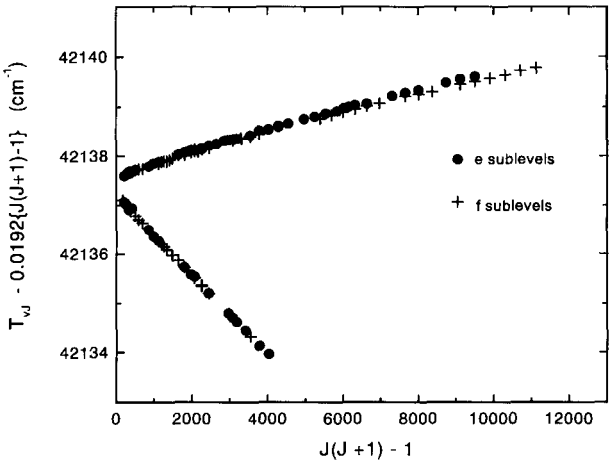

Fig. 5. Energy level diagram of the $1_u(^3P_2)$ $v = 5$ and $2_u(^3P_2)$ $v = 3$ states. Symbols showing the rotational levels are: (●) for the *e* sublevels observed through the P and R branches of the $A^3\Pi(1_u)$—$X^1\Sigma_g^+$ transition, and (+) for the *f* sublevels observed through the Q branches of the $A^3\Pi(1_u)$–$X^1\Sigma_g^+$ transition.

Figures 6 and 7 show two other examples involving the $2_u(^3P_2)$ state, which was found in the energy regions of the $1_u(^3P_2)$ $v = 6$ and 7 states, respectively. We attempted to identify the $2_u(^3P_2)$ state, though our observations were limited to the states in the energy range close to the avoided crossing. The $2_u(^3P_2)$ state does not couple with the $0_u^+(^3P_2)$ state due to the $\Delta\Omega = \pm 1$ selection rules for a perturbation. The Ω-doubling of the $2_u(^3P_2)$ state occurs through the $1_u(^3P_2)$ state, and it is by one order of magnitude smaller than that of the $1_u(^3P_2)$ state. The pattern of the Ω-doubling, therefore, follows that of the $1_u(^3P_2)$ state, which agrees with our observation. It should be pointed out here that the energy levels of the $2_u(^3P_2)$ state shown in Figs. 5, 6, and 7 closely

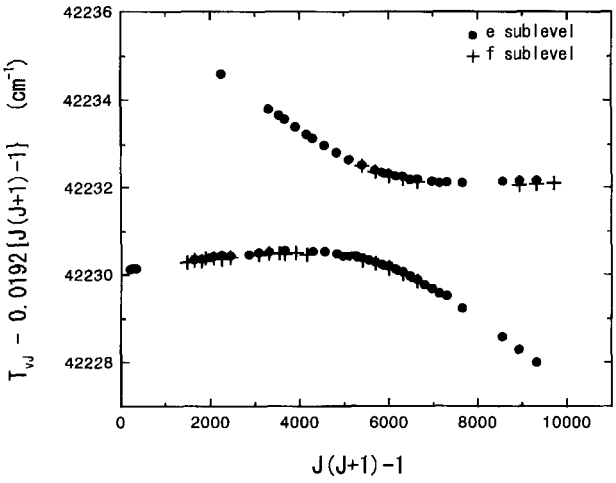

Fig. 6. Energy level diagram of the $1_u(^3P_2)$ $v = 6$ and $2_u(^3P_2)$ $v = 4$ states. Symbols showing the rotational levels are the same as in Fig. 5.

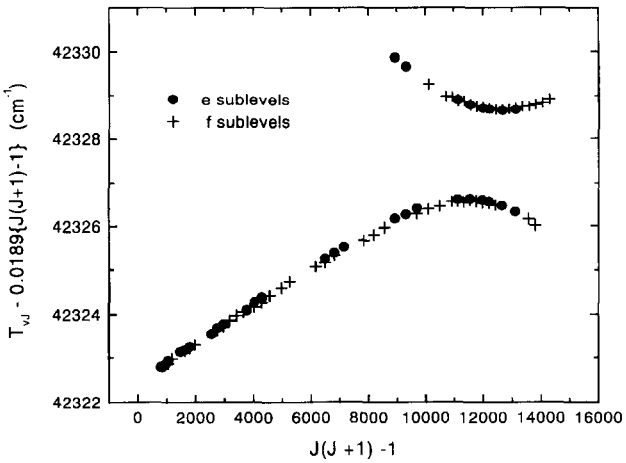

Fig. 7. Energy level diagram of the $1_u(^3P_2)$ $v = 7$ and $2_u(^3P_2)$ $v = 5$ states. Symbols showing the rotational levels are the same as in Fig. 5.

coincide with those of the δ state vibrationally numbered as $v = 3$—5 by King et al. in terms of their absolute positions. This finding supports the previous prediction that δ is the $2_u(^3P_2)$ state.

The term-value analyses of the ion-pair states were carried out using a computer program which took into account the following Hamiltonian matrix elements. The diagonal parts represent the energies of the $1_u(^3P_2)$ and $2_u(^3P_2)$ states:

$$\langle \Omega, vJ|H|\Omega, vJ\rangle = \sum Y_{lm}(v+1/2)^l\{J(J+1)-\Omega^2\}^m + \chi \cdot q_{lm}(v+1/2)^l\{J(J+1)-\Omega^2\}^m, \quad (3)$$

where χ is a switching parameter which should only be applied to the $1_u(^3P_2)$ state for taking account of the Ω-doubling. The value is +1 for *e* sublevels and 0 for *f* sublevels. The off-diagonal elements are

$$\langle \Omega+1, v'J|H|\Omega, vJ\rangle = -\beta_{v,v'}^{\Omega,\Omega+1}\{J(J+1)-\Omega(\Omega+1)\}^{1/2}. \quad (4)$$

The dimension of the appropriate energy matrix depends on the considered vibrational levels. In calculations of the energy range where the $1_u(^3P_2)$ $2 \leq v$ states were located, we took account of the 1_u–$2_u(^3P_2)$ interactions between the levels in near resonance. The 4×4 secular equation was symmetrically factorized into problems to solve a 2×2 determinant (*e* sublevels with $\Omega = 1$ and 2) and a 2×2 determinant (*f* sublevels with $\Omega = 1$ and 2), including the interaction matrix between the *v*-th vibrational level of the Ω state and the closely resonant *v'*-th level of the Ω' state. In addition to the interaction between the near resonant levels, the heterogeneous interaction matrix elements are also responsible for more distant interactions with other vibrational levels. However, these effects from the remote Ω', *v'* states to the *v*-th vibrational levels of the Ω state were neglected in the analysis and absorbed into the rotational constants. On the other hand, the $1_u(^3P_2)$ $v \leq 1$ states did not couple with the nearby $2_u(^3P_2)$ state, since they lie below the potential minimum of the $2_u(^3P_2)$ state. For these states, the dimension of energy matrix was 2×2, consisting of the diagonal matrix elements representing the energies of the $1_u(^3P_2)$ states.

Table 1. Molecular Constants of the $1_u(^3P_2)$ State of I_2[a)]

	This work	Reference 4
Y_{00}	41621.444(6)	41621.29(20)
Y_{10}	94.7389(38)	95.01(14)
Y_{20}	−0.17093(68)	−0.222(27)
Y_{30}	$1.92(37)\times10^{-4}$	
Y_{01}	0.0195863(11)	0.019702(27)
Y_{11}	−0.00002745(37)	−0.0000272(68)
Y_{21}	$-4.51(35)\times10^{-7}$	
Y_{02}	$-2.906(92)\times10^{-9}$	
q_{01}	$9.66(47)\times10^{-6}$	
q_{21}	$4.4(11)\times10^{-8}$	

a) In cm^{-1} and σ in parentheses.

The present analysis method can determine the interaction terms between the 1_u and $2_u(^3P_2)$ states from the energy shift of the $1_u(^3P_2)$ state and the positions of extra lines. The difficulty of the analysis lies in evaluating the 1_u–$2_u(^3P_2)$ coupling terms, which could not be solely determined from the spectroscopic data, except for the states shown in Figs. 5, 6, and 7. Consequently, the parameters for the 1_u–$2_u(^3P_2)$ interaction were first estimated from the pure precession values:[20]

$$\beta_{v,v'}^{\Omega,\Omega+1} = \eta_{\Omega,\Omega+1}^{el} \cdot B_{v,v'}^{\Omega,\Omega+1} = \langle \Omega+1|L_+ + S_+|\Omega\rangle\langle \Omega+1, v'|h/8\pi^2 c\mu r^2|\Omega, v\rangle, \quad (5)$$

where $\eta_{\Omega,\Omega+1}^{el} = \{J_a(J_a+1)-\Omega(\Omega+1)\}^{1/2} = 2$. The value of J_a denotes the total angular momentum of the I^+ ion in a separated atom basis set, $|I^+(^3P_J)m_j\rangle$ $|I^-(^1S)m_j\rangle$, representing the wavefunction of the ion-pair state; $J_a = 2$ and $\Omega = 1$ for the 1_u–$2_u(^3P_2)$ interaction.[20] The $B_{v,v'}^{\Omega,\Omega+1}$ factors can be numerically calculated from the RKR potential curves of two interacting states. The initial sets of the Dunham coefficients were estimated and the RKR curves were constructed using rotational parameters averaged between the *e* and *f* sublevels. On this basis, the $B_{v,v'}^{\Omega,\Omega+1}$ factors were calculated and fed to a least-squares fit program. The molecular parameters for the ion-pair states were then refined and reintroduced into calculations of the RKR potential curves to correct the perturbation terms. It is fortunate that this procedure does not cause any serious problem in analyzing the spectra. The interaction matrix elements were successfully determined in the vibrational states where the heterogeneous coupling was important to understand the energy levels. The fitting is excellent in any energy regions, and the standard deviation ($0.0175\ cm^{-1}$) is close to our experimental accuracy.

C. The $1_u(^3P_2)$ and $2_u(^3P_2)$ Ion-Pair States of I_2: Tables 1 and 2 summarize two sets of molecular constants obtained for the $1_u(^3P_2)$ and $2_u(^3P_2)$ states of I_2 together with those reported previously. Table 3 lists the 1_u–$2_u(^3P_2)$ heterogeneous interaction terms.

This study solved some restrictions of the previous experiments to access the $1_u(^3P_2)$ state through the high vibrational levels of the $B^3\Pi(0_u^+)$ state where parity mixing occurs. We were able to extend the observation of the rotational lev-

Table 2. Molecular Constants of the $2_u(^3P_2)$ State of I_2[a]

	This work	Reference 4
Y_{00}	41787.76(18)	41789
Y_{10}	100.695(93)	100.2
Y_{20}	−0.222(13)	−0.13
Y_{01}	0.018548(11)	0.0163
Y_{11}	−0.0000375(25)	
Y_{02}[b]	-2.46×10^{-9}	

a) In cm^{-1} and σ in parentheses. b) Fixed to the value $Y_{02} = -4Y_{01}^3/Y_{10}^2$.

Table 3. Interaction Matrix Elements ($\beta_{v,v'}^{\Omega,\Omega+1}$) between the $1_u(^3P_2)$ and $2_u(^3P_2)$ States

$1_u(^3P_2)$	$2_u(^3P_2)$	Obsd[a]	Calcd[b]
$v = 2$	$v = 0$	0.01331(77)	0.01482
3	1	0.01988(38)	0.01910
4	2	0.01966(28)	0.01932
5[c]	3	0.017557(82)	0.01687
6[c]	4	0.013767(28)	0.01279
7[c]	5	0.009720(11)	0.00793
8	6	0.00292[d]	0.00292
9	7	0.00174[d]	0.00174
10	8	0.00569[d]	0.00569
11	9	0.00873[d]	0.00873

a) In cm^{-1} and σ in parentheses. b) Calculated for $J = 1$.
c) The vibrational states where the extra lines were observed.
d) Fixed to the pure precession value.

els, and the molecular constants were greatly improved. In particular, it is important that the $1_u(^3P_2)$ state is shown to be degenerated. The excitation to the $1_u(^3P_2)$ state is also clear in the double-resonance spectra observed through the $A^3\Pi(1_u)$ state in view of the Franck–Condon factor consideration. For example, the Franck–Condon factors were calculated for the progression of the $1_u(^3P_2)$–$A^3\Pi(1_u)$ system seen in spectrum (a) of Fig. 1. In this calculation, we constructed the RKR potential of the $1_u(^3P_2)$ state using the constants in Table 1, and that of the $A^3\Pi(1_u)$ state using the constants of Appaddo et al. Without taking account of several correction terms such as (1) the effects of a heterogenous interaction, (2) the intensity distribution of the emission spectrum, and (3) the dependence of the transition moment on the internuclear axis, calculations using the effective potential for the correspond J levels can predict the intensity distribution of vibrational progressions reasonably well. This finding, together with the fact that the two-photon transition from the $A^3\Pi(1_u)$ state obeys the rotational selection rules between the states of $\Delta\Omega = 0$, makes the assignment of the ion-pair state as $1_u(^3P_2)$ unequivocal. Table 4 lists the potential curve of the $1_u(^3P_2)$ state for $J = 1$.

In the $1_u(^3P_2)$ state the e sublevels lie higher than the f sublevels. The Ω-doubling is caused by a heterogenous interaction with the $0_u^+(^3P_2)$ state correlating to same asymptote of $I^-(^1S)+I^+(^3P_2)$. Based on the potential curves of the ion-pair states correlating to $I^+(^3P_2)+I^-(^1S)$ summarized in Fig. 8, the $0_u^+(^3P_2)$ state is known to lie at an energy 592 cm^{-1} lower than that of $1_u(^3P_2)$ state. The $0_u^+(^3P_2)$ state interacts selectively with the e sublevels of the $1_u(^3P_2)$ state in view of the selection rule for the perturbation (+↔+ and −↔−); it is therefore easy to understand that the $0_u^+(^3P_2)$ state pushes up the e sublevels of the $1_u(^3P_2)$ state. Since the equilibrium internuclear distance of the $0_u^+(^3P_2)$ state is shorter than that of the $1_u(^3P_2)$ state, the Ω-doubling of the $1_u(^3P_2)$ state shows a slight v dependence. The Ω-doubling constant is expressed by second-order perturbation theory,

Table 4. RKR Turning Points of the $1_u(^3P_2)$ State[a]

v	T_v (cm^{-1})	Turning points (Å)	
		Inner	Outer
0	47.307	3.60967	3.75954
1	141.705	3.55791	3.81790
2	235.762	3.52317	3.85934
3	329.481	3.49549	3.89385
4	422.861	3.47194	3.92432
5	515.905	3.45121	3.95209
6	608.614	3.43256	3.97790
7	700.988	3.41553	4.00220
8	793.029	3.39980	4.02531
9	884.738	3.38517	4.04744
10	976.116	3.37146	4.06876
11	1067.164	3.35854	4.08940

a) $r_e = 3.68305$ Å.

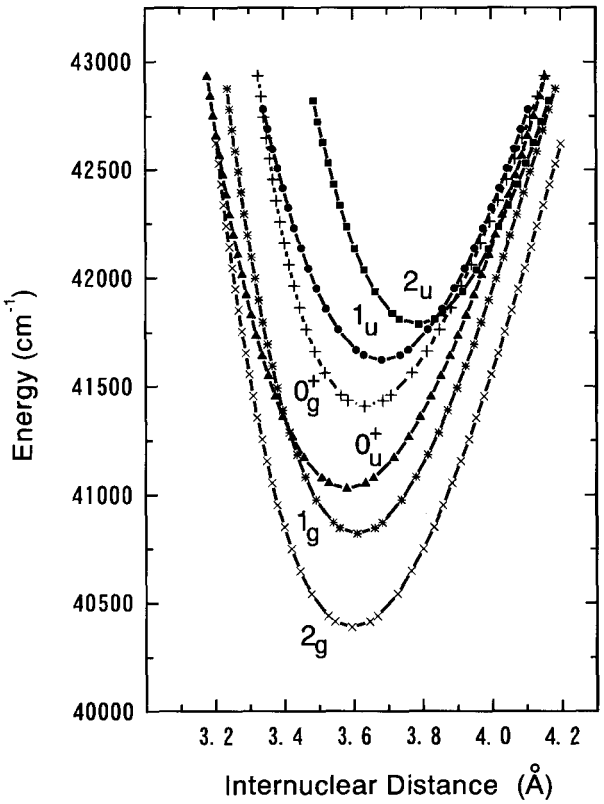

Fig. 8. Potential curves of the ion-pair states of I_2 correlating with $I^+(^3P_2)+I^-(^1S)$. 0_g^+; —+—, 1_g; —*—, 2_g; —×—, 0_u^+; —▲—, 1_u; —●—, and 2_u; —■—.

$$q_v = B_v^e - B_v^f = 2(\eta_{\Omega,\Omega+1}^{el})^2 \sum_{v'} \{\langle \Omega+1, v|h/8\pi^2 c\mu r^2|\Omega, v'\rangle^2/\Delta_{v,v'}\}, \quad (6)$$

where the value of $\Delta_{v,v'}$ is the energy difference between two vibrational levels, the v-th vibrational level of the $1_u(^3P_2)$ state and the v'-th level of the $0_u^+(^3P_2)$ state. We calculated the summation of the vibrational part in the $0 \leq v' \leq 40$ range for the $0_u^+(^3P_2)$ state while assuming $(\eta_{\Omega,\Omega+1}^{el})^2 = 6$ under the pure precession approximation. The thus-obtained values can be approximated by $q_v = \{9.52 + 0.0415(v+1/2)^2\} \times 10^{-6}$ cm^{-1} in the $v = 0$—11 range of the $1_u(^3P_2)$ state, which is in good agreement with our experimental values.

The vibrational numbering of the $2_u(^3P_2)$ state was readily established by comparing the matrix elements observed for the 1_u–$2_u(^3P_2)$ interaction with those calculated by the pure-precession model. The lowest vibrational state, where the 1_u–$2_u(^3P_2)$ interaction was identified by the occurrence of extra lines, was $v = 5$ of the $1_u(^3P_2)$ state. King et al. have observed three other vibrational levels of the $2_u(^3P_2)$ state below this energy region, and tentatively numbered the first observed level as $v = 0$. The calculation was first carried out assuming that the $v = 3$ level of the $2_u(^3P_2)$ state is in near-resonance with the $1_u(^3P_2)$ $v = 5$ state according to the vibrational numbering on the $2_u(^3P_2)$ state by King et al. This vibrational scheme provided the q_v values, which were very close to our observations, as shown in Table 3. In this calculation, we used the potential functions of the $1_u(^3P_2)$ and $2_u(^3P_2)$ states for the lowest rotational state. One reason for the larger deviations in the $1_u(^3P_2)$ $v = 6$ and 7 states is that the vibrational part in Eq. 4 shows a slight J dependence. The $\beta_{vv'}^{\Omega\Omega'}$ values at $v = 6$ and 7 of the $1_u(^3P_2)$ state were dominantly determined in the energy levels where the avoided crossing occurred, as shown in Figs. 6 and 7. Actually, the $\beta_{vv'}^{\Omega\Omega'}$ values, 0.01319 cm^{-1} calculated at $v = 6$ $J = 77$ and 0.00897 cm^{-1} at $v = 7$ $J = 110$, are found to be much closer to the observed values.

We further continued the calculations by adjusting the molecular parameters to shift the potential function to a lower energy and to a slightly shorter equilibrium internuclear distance in accordance with an increase of the vibrational numbering of the $2_u(^3P_2)$ state. A decrease in the vibrational numbering is meaningless due to the observation by King et al. The 1_u–$2_u(^3P_2)$ interaction terms showed a strong dependence on the vibrational scheme, and the observed values were not reproduced in these calculations. These results leave no doubt about the vibrational numbering of the $2_u(^3P_2)$ state proposed by King et al. in view of the consistency of the observed to calculated values of the interaction matrix elements.

Conclusions

The $1_u(^3P_2)$ ion-pair state of I_2 was located by optical-optical double resonance using the $A^3\Pi(1_u)$ state as an intermediate. We have rotationally analyzed this state in the $0 \leq v \leq 11$ and $5 \leq J \leq 119$ ranges. Three vibrational levels ($3 \leq v \leq 5$) of the $2_u(^3P_2)$ state were also detected by intensity borrowing from the $1_u(^3P_2)$ state through heterogenous mixing. This study unambiguously indicates that the γ and δ states observed by Danyluk and King are identical to the $1_u(^3P_2)$ and $2_u(^3P_2)$ state, respectively, and leads to much improved spectroscopic descriptions of these excited states.

The data presented here finally establish a map of the six ion-pair states of I_2 correlating with $I^+(^3P_2)+I^-(^1S)$, as shown in Fig. 8. The $2_g(^3P_2)$ state responsible for the laser oscillation at 340 nm is located at the lowest energy, and the $1_g(^3P_2)$ and $0_g^+(^3P_2)$ states follow to lie above the $2_g(^3P_2)$ state. These three *gerade* states have been characterized with reasonable accuracy, showing a close family-likeness in their potential functions. On the other hand, we find that three *ungerade* states, 0_u^+, 1_u, and $2_u(^3P_2)$, are located in order of increasing energy and that their potential functions are not uniform in reflecting the scattering of the vibrational and rotational constants.

The authors are grateful for a Hiroshima City University Grant for Special Academic Research (General Studies).

References

1 J. C. D. Brand and A. R. Hoy, *Appl. Spectrosc. Rev.*, **23**, 285 (1987).
2 D. L. Rousseau and P. F. Williams, *Phys. Rev. Lett.*, **33**, 1368 (1974).
3 M. D. Danyluk and G. W. King, *Chem. Phys.*, **22**, 59 (1977).
4 G. W. King, I. M. Littlewood, and J. R. Robins, *Chem. Phys.*, **56**, 145 (1981).
5 J. C. D. Brand, A. R. Hoy, A. K. Kalkar, and A. B. Yamashita, *J. Mol. Spectrosc.*, **95**, 350 (1982).
6 J. P. Perrot, M. Broyer, J. Chevaleyre, and B. Femelat, *J. Mol. Spectrosc.*, **98**, 161 (1983).
7 J. C. D. Brand, A. R. Hoy, and D. C. P. Tse, *Can. J. Spectrosc.*, **30**, 40 (1985).
8 J. P. Perrot, B. Femelat, J. L. Subtil, M. Broyer, and J. Chevaleyre, *Mol. Phys.*, **61**, 97 (1987).
9 J. Tellinghuisen, *J. Chem. Phys.*, **78**, 2374 (1983).
10 J. Tellinghuisen, *J. Mol. Spectrosc.*, **137**, 248 (1989).
11 X. Zheng, S. Fei, and M. C. Heaven, and J. Tellinghuisen, *J. Chem. Phys.*, **96**, 4877 (1992).
12 K. S. Viswanathan and J. Tellinghuisen, *J. Mol. Spectrosc.*, **101**, 285 (1983).
13 M. Broyer, J. Vigue, and J. C. Lehmann, *J. Phys.*, **39**, 591 (1978).
14 J. Tellinghuisen, *Chem. Phys. Lett.*, **99**, 373 (1983).
15 A. D. William and R. N. Compton, *Chem. Phys. Lett.*, **62**, 295 (1979).
16 T. Ishiwata and I. Tanaka, *Laser Chem.*, **7**, 79 (1987).
17 D. R. T. Appadoo, R. J. Le Roy, P. F. Bernath, S. Gerstenkorn, P. Luc, J. Verges, J. Chevillard, and Y. D'Aignaux, *J. Chem. Phys.*, **104**, 903 (1996).
18 W. M. McClain and R. A. Harris, "Excited States," ed by E. C. Lim, Academic Press, New York (1978), Vol. 1, p. 1.
19 P. J. Jewsbury, T. Ridley, K. Lawley, and R. J. Donovan, *J. Mol. Spectrosco.*, **157**, 33 (1993).
20 D. Bussieres and A. R. Hoy, *Can. J. Phys.*, **62**, 1941 (1984).